J Muscle Res Cell Motil (2008) 29:25–36
DOI 10.1007/s10974-008-9139-8

ORIGINAL PAPER

Mice expressing L345P mutant desmin exhibit morphological and functional changes of skeletal and cardiac mitochondria

Anna Kostareva · Gunnar Sjöberg · Joseph Bruton · Shi-Jin Zhang · Johanna Balogh · Alexandra Gudkova · Birgitta Hedberg · Lars Edström · Håkan Westerblad · Thomas Sejersen

Received: 23 October 2007 / Accepted: 28 May 2008 / Published online: 19 June 2008

Abstract Desmin mutations underlie inherited myopathies/cardiomyopathies with varying severity and involvement of the skeletal and cardiac muscles. We developed a transgenic mouse model expressing low level of the L345P desmin mutation (DESMUT mice) in order to uncover changes in skeletal and cardiac muscles caused by this mutation. The most striking ultrastructural changes in muscle from DESMUT mice were mitochondrial swelling and vacuolization. The mitochondrial Ca^{2+} level was significantly increased in skeletal and cardiac myocytes from DESMUT mice compared to wild type cells during and after contractions. In isolated DESMUT soleus muscles, contractile function and recovery from fatigue were impaired. A SHIRPA screening test for neuromuscular performance demonstrated decreased motor function in DESMUT compared to WT mice. Echocardiographic changes in DESMUT mice included left ventricular wall hypertrophy and a decreased left ventricular chamber dimension. The results imply that low levels of L345P desmin acts, at least partially, by a dominant negative effect on mitochondria.

Keywords Desmin · Mutation · Mice · Mitochondria · Calcium · Muscle

Abbreviations

DESMUT	Mice transgenic with L345P mutated desmin
WT	Wild type mice

Introduction

Desmin is a major intermediate filament protein of muscle tissue, expressed in all three types of muscle cells: skeletal, cardiac and smooth (Lazarides 1980). Being one of the Z-disk associated proteins in striated muscles it encircles the myofibrils at the level of the Z-line and connects them to the plasma and nuclear membranes. In cardiomyocytes desmin participates in formation of costameres and intercalated disks. It is also known to be tightly associated with various intracellular organelles and structures, such as mitochondria and thin filaments (Lazarides 1982). Indeed in desmin null mice, mitochondrial function is markedly impaired (Milner et al. 2000). During contraction, desmin assists in the simultaneous shortening of different myofibrils and facilitates force transmission along the cell minimizing shear stress. Finally, desmin has been shown to be involved in signal transduction and apoptosis (Chen et al. 2003; Ingber 1997).

Desmin mutations are implicated in several skeletal and cardiac disorders. Desmin-positive inclusions were noted

A. Kostareva · G. Sjöberg · T. Sejersen (✉)
Department of Woman and Child Health and Center for Molecular Medicine, Karolinska Institute, L8:02, Stockholm 17176, Sweden
e-mail: thomas.sejersen@cmm.ki.se

A. Kostareva · A. Gudkova
Department of Faculty Therapy, Pavlov Medical University, Saint Petersburg 197022, Russia

J. Bruton · S.-J. Zhang · H. Westerblad
Department of Physiology and Pharmacology, Karolinska Institute, Stockholm 17177, Sweden

J. Balogh
Department of Physiological Sciences, University of Lund, Lund 22184, Sweden

B. Hedberg · L. Edström
Department of Neurology, Karolinska Institute, Stockholm 17176, Sweden

first in inherited distal myopathies with protein accumulations (Barohn 1993; Fidzianska et al. 1999). Subsequently, the first genetic identification of a desmin mutation was described in a patient with distal inherited myopathy (Munoz-Marmol et al. 1998). Later, Li et al. (1999) described a missense mutation in the desmin gene as a cause of dilated cardiomyopathy without skeletal muscle involvement. Since then, a total of 27 desmin mutations have been identified giving rise to either discrete skeletal or cardiac myopathy or most commonly, a concomitant skeletal-cardiac phenotype (Fidzianska et al. 2005; Goldfarb et al. 2004). Currently, genotype-phenotype correlations are poorly understood.

Earlier, we reported a L345P desmin mutation in a six-generation Ashkenazi family (Sjöberg et al. 1999). The mutation is located in the 2B part of the desmin rod domain, which is known to be important in filament formation and the polymerization process (Herrmann et al. 2000; Strelkov et al. 2002). This missense mutation has a dominant-negative effect on filament formation resulting in desmin malformations and characterized by myopathy and cardiomyopathy. We constructed a transgenic mouse model, carrying a L345P desmin mutation driven by a native desmin promoter in order to mimic normal desmin expression pattern in skeletal muscle and heart. Our primary aim was to identify the early specific skeletal and cardiac muscle dysfunctions resulting from the L345P desmin mutation. We were particularly interested in changes in mitochondrial and contractile function. Our animals displayed a relatively low level of expression of mutant desmin. Despite this, we found marked changes in mitochondrial structure and function.

Material and methods

DNA constructs and generation of transgenic mice

Animal care and experiments were approved by the Stockholm North local animal ethics committee. The T to C mutation in codon 345, causing an amino acid change from leucine to proline (L345P), was introduced into the mouse desmin cDNA by site-directed mutagenesis (QuikChange™ from Stratagene). From in vitro experiments we know that this mutation causes severe alteration of the desmin polymerization process (Bär et al. 2005). We tagged the desmin construct at the 5′ end with a hemagglutinin sequence (HA tag) of 30 nucleotides coding for the amino acid sequence YPYDVPDYAS, which is specifically recognized by a HA antibody. A poly A tail was finally attached to the desmin 3′ end and the whole construct was inserted downstream of the 4 kB mouse desmin promoter (kind gift of Dr. Denise Paulin; see Fig. 1c). The desmin

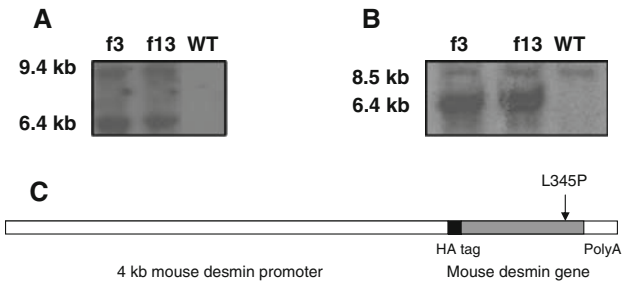

Fig. 1 Southern blot analysis of mouse genomic DNA for L345P desmin transgene. (**a**) Hybridization with a 500 bp probe, covering exon–exon borders of desmin gene. WT desmin is not detected with this probe. Positive hybridization in founder 3 and founder 13. L345P transgenes, located as tandem repeats correspond to the 6.4 kb band and L345P transgenes, located at the ends of tandem repeats correspond to the 9.4 kb band. Note absence of L345P transgenes in WT mice. (**b**) Hybridization with a 460 bp probe, containing the mouse desmin exon 1 sequence. This probe recognizes both mutated and wild-type desmin. Positive 8.5 kb signal from hybridization with WT desmin and the 6.4 kb signal from hybridization with L345P desmin. Negative control (WT mice) contains only WT desmin gene copies. The ratio between WT and L345P desmin is 1:10 for founder 3 and 1:8 for founder 13. (**c**) Schematic drawing of the transgenic construct. The mutation was introduced by site-directed mutagenesis and a hemagglutinin (HA) tag was placed at the N-terminus of the gene. This construct was then inserted distal to the 4 kB terminal part of the mouse desmin promoter

gene and promoter was then cleaved out from the cloning vector and purified for introduction into J-129 mouse pronuclei. Stable transgenic line (DESMUT mice) was established by mating with C57 Bl/6 mice. Wild type animals (C57 Bl/6) were used as a control (WT mice). For all experimental procedures animals were killed by cervical dislocation.

Genomic DNA analysis

Genotyping analysis

Total genomic DNA was extracted from tail tips after overnight incubation in lysis buffer, containing 0.2 M NaCl, 0.1 M Tris 8.3, 5 mM EDTA, 0.2% SDS and 100 mg of proteinase K. Primers, covering the HA sequence and the exon–exon borders were used for genotyping by PCR reaction.

Southern blot analysis

Following overnight digestion with EcoR1, mouse genomic DNA was separated by size on an agarose gel and transferred to a nylon membrane according to a standard protocol. In order to confirm the transgenic status of the founder animals, a membrane was hybridized with a 500 bp P^{32}-labeled probe, covering the exon–exon borders of the mouse desmin gene, allowing the distinction of

transgenic desmin construct from the wild type gene. For identification of transgene copy numbers, DNA from different founders was hybridized with a 460 bp P^{32}-labeled probe containing the exon 1 sequence of mouse desmin gene. To determine the ratio between wild type and transgenic copy number, images were obtained with an isotope scanning camera (Fujifilm, Tokyo, Japan) and quantification was performed using ImageGuard 3.45 software.

Western blot analysis

Tissue samples were homogenized on ice in intermediate filament suspension buffer, containing phosphate buffered saline (PBS, pH 7.4), 1% Triton X, 5 mM EDTA and protease inhibitors. After centrifugation at 4°C, the supernatant (containing the soluble desmin fraction) was removed and saved. The remaining pellet was resuspended in SDS-PAGE loading buffer, boiled, centrifuged, and the supernatant (containing the insoluble filamentous desmin fraction) was saved. Both soluble and insoluble fractions were run on a 10% SDS-polyacrylamide gel, followed by transfer to a nitrocellulose membrane. For detection of desmin, the membrane was incubated overnight at 4°C with an anti-desmin polyclonal antibody (DAKO), diluted 1:6,000 in blocking solution. This was followed by washing in TBS-0.1% Tween and incubation with a secondary anti-rabbit-HRP conjugated antibody (1:10,000) for 1 h at room temperature. For detection of the HA-tag, rat monoclonal anti-HA antibodies conjugated to HRP (Roche) diluted to 5 mU/ml were applied to the membrane for 1 h at room temperature. After washing the membranes in TBS-0.1% Tween, the signal was detected by Enhanced Chemi Luminescence Advance (Amersham Pharmacia Biotech) and visualized with a CCD camera (Fujifilm, Tokyo, Japan). All quantifications were done using ImageGuard 3.45 software.

The relative amount of total protein was estimated by staining the membrane in Ponceau reagent with subsequent destaining in distilled water and blocking in 8% non-fat milk in TBS-0.1% Tween. Signal intensity from antibody stained membranes were recalculated in the computer program according to minor difference in protein loading, visualized by Ponceau.

Tissue preparation and morphological examination

Tissue samples for light microscopy were immediately excised, washed in PBS, mounted in Tissue Tec, and frozen in liquid nitrogen. Separate samples from the left ventricle lateral wall, right ventricle and interventricular septum were obtained. For skeletal muscle examination cross sections of soleus, tibialis anterior, extensor digitorum longus (EDL), and diaphragm were used. Conventional staining with hematoxyline–eosin for skeletal and cardiac muscles was performed according to standard protocols. Sections were examined using Zeiss Axioscop 2 microscope with a 20× or 40× lens.

Electron microscopy was performed on samples from the left ventricle, tibialis anterior and soleus muscles. After fixation in 3% glutaraldehyde in phosphate buffer samples were cut in blocks approximately 1 mm × 0.5 mm and postfixed in OsO4 in PBS, dehydrated in alcohol and embedded in LX-112. Semi-thin sections (0.5 μm) were stained with toluidine blue. Areas of interest were selected for ultrathin sections (60–70 nm) and contrasted with uranyl acetate and lead citrate. Sections were examined in a 1235 Jeol transmission electron microscope (Jeol Ltd., Tokyo, Japan) at 60 kV. For each tissue sample, a minimum of four sections were studied and three animals from each group were examined.

Immunohistochemistry

Cryosections of heart and skeletal muscles were air-dried, blocked with 15% goat serum at room temperature for 1 h, and incubated overnight at 4°C with a primary anti-desmin polyclonal antibody (Sigma) diluted 1:40 in blocking solution. After being washed in PBS, sections were incubated with an anti-rabbit FITC-conjugated secondary antibody (Sigma), diluted 1:200 in blocking solution for 1 h at room temperature. For detection of tissue macrophages sections were incubated with anti-CD68 rat monoclonal (Santa Cruz) antibody for 1 h at room temperature with subsequent staining with HRP-conjugated goat anti rat secondary antibody followed by DAB staining visualization. Sections (10 μm) were examined on a Zeiss Axioscop 2 microscope.

Measurement of mitochondrial Ca^{2+}

Mice were killed and the heart or soleus muscle was excised. Single cardiomyocytes were enzymatically isolated from the ventricles as described previously (Fauconnier et al. 2005). Mitochondria were loaded with the Ca^{2+}-sensitive dye rhod-2 as follows. Cardiomyocytes were incubated in 5 μM rhod-2-AM (Molecular Probes) for 60 min at 4°C and then washed for 20 min at 24°C. Single intact muscle fibres were mechanically dissected from the soleus muscle (Bruton et al. 2003). Soleus fibres were incubated in 5 μM rhod-2-AM (Molecular Probes) for 120 min at 24°C and then washed for 30 min. A BioRad MRC 1024 and a Nikon Diaphot 200 inverted microscope with a Nikon Plan Apo 40× oil immersion objective lens (N.A. 1.3) were used. Rhod-2 was excited with 568 nm light and the emitted light collected through a 585 nm

long-pass filter. Confocal images were taken of the muscle fibres at rest and then at regular intervals during and after a series of contractions. Confocal images were stored and analysed offline with ImageJ (available at http://rsb.info.nih.gov/ij/). Changes in mitochondrial rhod-2 intensity at each time point (F) were expressed as a ratio of that measured in the rested fibre (F_0). This procedure allowed comparison of the mitochondrial rhod-2 signal in different cells.

Skeletal muscle contractile function

The contractile function was studied in isolated skeletal muscles from 70 weeks old female WT and DESMUT mice. Animals were killed and the soleus and the fast-twitch EDL muscles were removed. Muscles were mounted in the stimulation chambers in Tyrode solution at 25°C. The muscle length was adjusted to that giving maximum tetanic force response. Muscles were then allowed to rest for 30 min. The force–frequency relationship was obtained as described earlier (Belluardo et al. 2001). After the force–frequency relationship, fatigue was produced with intermittent tetani contractions and finally the extent of force recovery was monitored for 30 min after fatigue.

Behavioural and functional analysis

The SHIRPA primary screening protocol (Rafael et al. 2000) was used for behavioural and phenotypic assessment of the mice (for further details see http://www.mgu.har.mrc.ac.uk/mutabase/shirpa). Within the SHIRPA protocol, the wire manoeuvre test is the most important to asses hind limb function. In this test, a suspended mouse is allowed to grasp the metallic wire with its fore limbs and is then released. Animals are expected to grasp the wire with their hind-legs immediately or within several seconds. Mutant and control groups ($n = 10$ in both cases) were examined at different ages. The protocol was performed blind, with the examiner being unaware of the mouse's identity.

Echocardiography and electrocardiography

Animals were anesthetized with 1.2% isoflurane and maintained on a heated platform. Two-dimensional guided M mode images were obtained at the level of papillary muscles using a Philips ATL HTI5000E echocardiograph equipped with a 15 MHz probe, CL 15-7. Parameters were averaged over several cardiac cycles. Left ventricular end-systolic (LVESD) and end-diastolic (LVEDD) diameters as well as systolic (LVPWs) and diastolic (LVPWd) posterior wall thickness were measured using leading edge-to-leading edge convention. Left ventricular fractional shortening (FS) was calculated as $[(\text{LVEDD} - \text{LVESD})/\text{LVEDD}] \times 100\%$. ECG was recorded simultaneously with two-lead limb connections. Baseline recordings were obtained for 15 min before starting echocardiography. ECG analysis was performed with PcLaB 5.0 software.

Statistical analysis

Data were obtained from indicated number of mice and expressed as mean ± SEM. Statistical significance between DESMUT and WT groups were analyzed using a Student's t-test. Statistical analysis of SHIRPA protocol was performed by using one-sided Fisher's exact test. In all tests, the level of significance was set as $P < 0.05$.

Results

Generation of transgenic mice expressing L345P mutant desmin (DESMUT mice)

Totally five transgenic founders expressing HA-tagged L345P desmin were identified by PCR genotyping and T to C substitution was confirmed by DNA sequencing. Based on the results of Southern blot (see Fig. 1) and Western blot (data not shown), the two founders with the highest number of transgene copies and level of transgene expression were chosen for further experimental studies (f3 and f13, Fig. 1a). The ratio between L345P and wild type (WT) desmin gene copies was 10 for f3 and 8 for f13 (Fig. 1b). Further genotyping of the subsequent litters was done using PCR only. The DESMUT mice had a life span similar to WT animals. Their litter sizes were normal and the body weight did not differ from the control group at any of the studied time points (Table 1).

Mutant desmin protein is expressed at low level in transgenic animals

In DESMUT mice, expression of L345P desmin was detected in all analysed muscle tissues, except for the urinary bladder (Fig. 2b). However, in all muscles examined the average expression level of L345P desmin was

Table 1 Body weight (g) of male and female wild type (WT) and desmin mutant (DM) mice

	Males		Females	
	WT ($n = 6$)	DM ($n = 6$)	WT ($n = 10$)	DM ($n = 13$)
25 weeks	37.7 ± 1.0	36.5 ± 1.4	26.6 ± 1.4	28.8 ± 1.0
39 weeks	43.9 ± 1.8	43.7 ± 2.5	32.4 ± 1.8	33.7 ± 1.3
77 weeks	48.8 ± 1.1	46.3 ± 2.6	40.5 ± 1.9	38 ± 1.6

Values are mean ± SEM

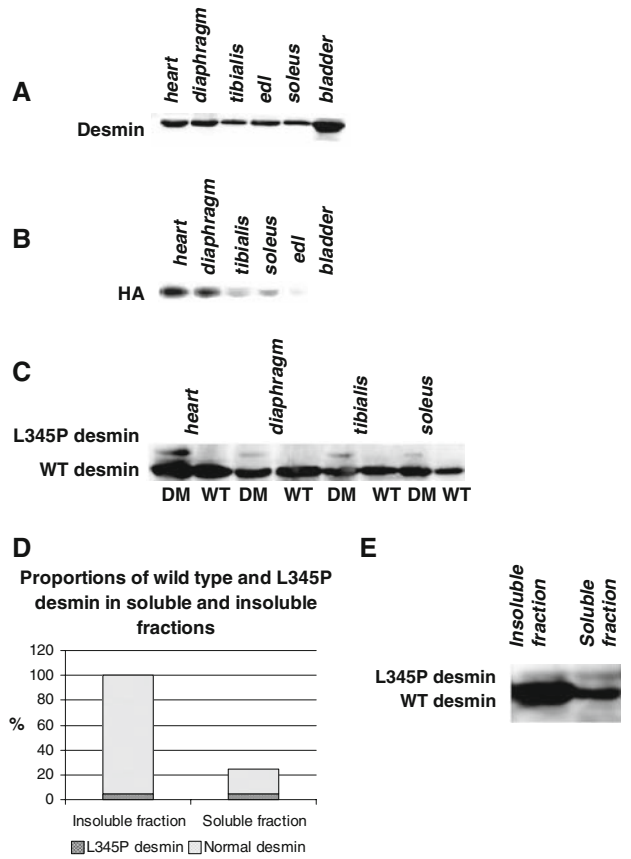

Fig. 2 Western blot analysis of muscle tissue from DESMUT mice. (**a**) Expression of WT desmin (anti desmin polyclonal antibody) in heart, skeletal muscles and urinary bladder. Insoluble protein fraction of WT mice. (**b**) Expression of HA-tag (anti HA monoclonal antibody), linked to transgenic L345P desmin, detected in all studies muscle tissues of DESMUT mice except for bladder. Insoluble protein fraction of transgenic animals. (**c**) Expression of WT and transgenic L345P desmin (anti desmin polyclonal antibody) in insoluble protein fraction of DESMUT mice. Transgenic desmin detected as higher molecular weight protein due to HA tag. The level of L345P desmin in the insoluble fraction is approximately 5 ± 0.3% of WT desmin in all studied muscle tissues. (**d**) Proportions of WT and L345P desmin in soluble and insoluble fractions of heart protein extracts from DESMUT mice. One hundred percent is defined as the total staining intensity of both mutated and wild type desmin in the insoluble fraction. (**e**) Expression of WT and L345P desmin in soluble and insoluble fractions of heart muscle from DESMUT mice

low (Fig. 2c) and constituted 5.0 ± 0.3% of the WT desmin in the insoluble fraction. This low level was independent on founder and animal age. However, in the soluble protein fraction the level of L345P desmin was significantly higher being 17.4 ± 1.5% of that of WT desmin ($P < 0.05$, Fig. 2d). The overall level of WT desmin expression did not differ between DESMUT and WT groups. The expression of L345P desmin was highest in the heart and diaphragm, a pattern similar to WT desmin expression in striated muscle (Fig. 2a and b).

Mild morphological aberrations but absence of desmin aggregates in DESMUT mice

In desmin myopathy, accumulation of desmin aggregates and streaming of the Z line in muscle biopsies are often observed (Goldfarb et al. 2004). However in the present study immunostaining of all skeletal and cardiac muscles with anti-desmin antibody revealed no detectable difference in the pattern or intensity of staining between DESMUT and WT mice (Fig. 3). In DESMUT mice a regular cross-striated intermediate filament pattern with no desmin aggregates was observed in heart and skeletal muscle, similar to that observed in WT mice. In DESMUT heart samples, anti-desmin antibody showed that desmin was also clearly localized to the intercalated discs. We could not detect any difference in the intensity of Z-line desmin staining or background non-Z-line associated staining between DESMUT and WT mice.

Despite the absence of desmin aggregates, other subtle morphological alterations of heart muscle were noted. In DESMUT mice there was an increased interstitial cellularity due to non-myogenic cells, minor perivascular oedema and focal myocytolysis together with cardiomyocyte disorganization (Fig. 4b). Cell infiltrations were observed in perivascular and intermyocyte spaces. The most typical feature of the cardiac muscle in the DESMUT group was local accumulation of protein depositions in foci of muscle fibre disruption, in perivascular spaces and in the extracellular matrix (arrows in Fig. 4c). The latter were accompanied by interstitial non-myogenic cell and macrophage infiltration and caused a disruption of overall tissue architecture (Fig. 4c and d). Additionally, Sirius red staining indicate increased fibrosis in the hearts of DESMUT mice (Fig. 4e and f). Cardiomyocyte disorganization varied from mild to moderate, being more prominent in areas of fibre disruption and protein depositions. These findings were found both in left and right ventricles, sometimes being even prevailing in the latter and were consistent in all animals analysed from DESMUT group.

Morphological examination of skeletal muscle in DESMUT animals showed no obvious pathological signs. There were no signs of muscle atrophy, dystrophy, inflammation, degeneration/regeneration, or fibrosis.

Electron microscopy revealed severe mitochondrial abnormalities in DESMUT mice

Electron microscopy examination of DESMUT heart, soleus, and tibialis anterior muscle, revealed no signs of myofibrillar major disturbance or misalignment. Sarcomere structure was normal, showing regular and non-streamed Z- and M-lines. The most striking changes appeared in the mitochondria of skeletal and cardiac muscles. These

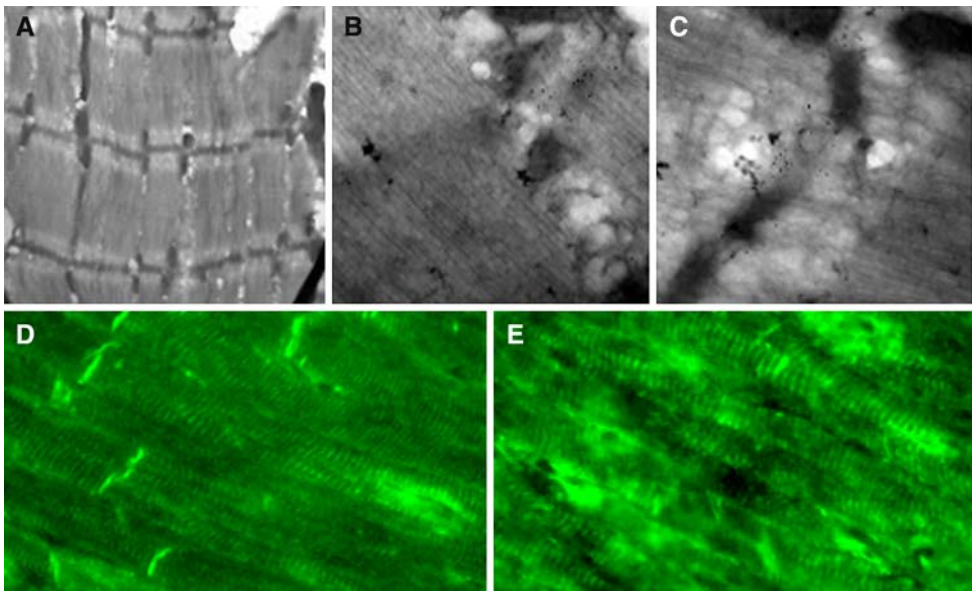

Fig. 3 Immuno-detection of desmin in left ventricular heart tissue from DESMUT and WT mice (**a**) Overview electron micrograph of section from DESMUT mouse illustrating normal Z-line structure of the sarcomeres. 30,000× (**b**) Immuno-EM staining of DESMUT mouse using gold conjugated anti-desmin antibodies. Note that the gold particles are localized at the Z-lines (arrows). 80,000× (**c**) Anti-desmin immuno-EM staining of WT mouse. Arrows indicate Z-line. 80,000× (**d**) Anti-desmin immunofluorescence staining of DESMUT left ventricle. 2,000× (**e**) Anti-desmin immunofluorescence staining of WT left ventricle. 2,000×

changes included reduced cristae density (Fig. 5c) and significant vacuolization of mitochondrial matrix resulting in the formation of circular membrane structures (Fig. 5d), and giant mitochondria (Fig. 5f). Groups of abnormal mitochondria usually appeared as clusters, together with pools of mitochondria of normal appearance. In such areas, there were altered myofibril distribution and thinning of myofibrils (Fig. 5b). In such cases the inter-myofibrillar space was filled with amorphous unstructured material (Fig. 5e). All of these changes were consistently observed in all samples from both cardiac and skeletal muscle of DESMUT mice, and were not present in WT mice.

Abnormal Ca^{2+} handling by mitochondria in skeletal and cardiac muscle cells

Structural and functional changes of mitochondria have been suggested to be caused by excessive mitochondrial Ca^2 loading in many cell types (Bernardi 1999). Thus, we decided to study mitochondrial Ca^{2+} uptake in DESMUT animals. Mitochondrial Ca^{2+} increased in both DESMUT and WT soleus muscle fibres. Figure 6a shows that during a series of 500 tetani, mitochondrial Ca^{2+} increased and reached its peak value after 50 tetani (DESMUT 4.1 ± 0.3 versus WT 2.7 ± 0.7). Thereafter mitochondrial Ca^{2+} decreased by about 30–40% during the remainder of the series of 500 tetani in both groups. However, even at the end of the period of stimulation, mitochondrial Ca^{2+} was more than 80% greater in DESMUT compared to WT soleus muscle fibres. Mitochondrial Ca^{2+} returned more slowly to its resting level in DESMUT than in WT fibres.

A similar alteration in mitochondrial Ca^{2+} handling was seen also in DESMUT cardiomyocytes during 1 min of stimulation at 1 Hz. The increase in calcium uptake in DESMUT cardiomyocytes was twice that measured in WT cardiomyocytes (Fig. 6b). Five minutes after the end of stimulation, mitochondrial Ca^{2+} had returned to its initial value in WT cardiomyocytes, but remained significantly elevated in DESMUT cardiomyocytes. Thus, during stimulation, the increase in mitochondrial Ca^{2+} is more pronounced and is less readily reversed in DESMUT compared to WT cardiomyocytes. In conclusion, stimulation induced increases in mitochondrial Ca^{2+} in both skeletal and cardiac myocytes that were greater and slower to reverse in DESMUT than in WT fibres.

Contractile function of isolated skeletal muscle in DESMUT mice

Muscle weight was not significantly different in DESMUT compared to WT mice. In the soleus, absolute tetanic force at 70 Hz did not significantly differ in DESMUT and WT mice (171 ± 36 and 193 ± 8 mN, respectively, $P > 0.05$). Relative force at 1, 15 and 20 Hz was significantly lower in DESMUT compared to WT (Fig. 7a, $P < 0.05$). During the induction of fatigue with 100 tetani (600 ms, 50 Hz tetani given every 2 s), there was no significant difference in tetanic force between DESMUT and WT soleus (Fig. 7b).

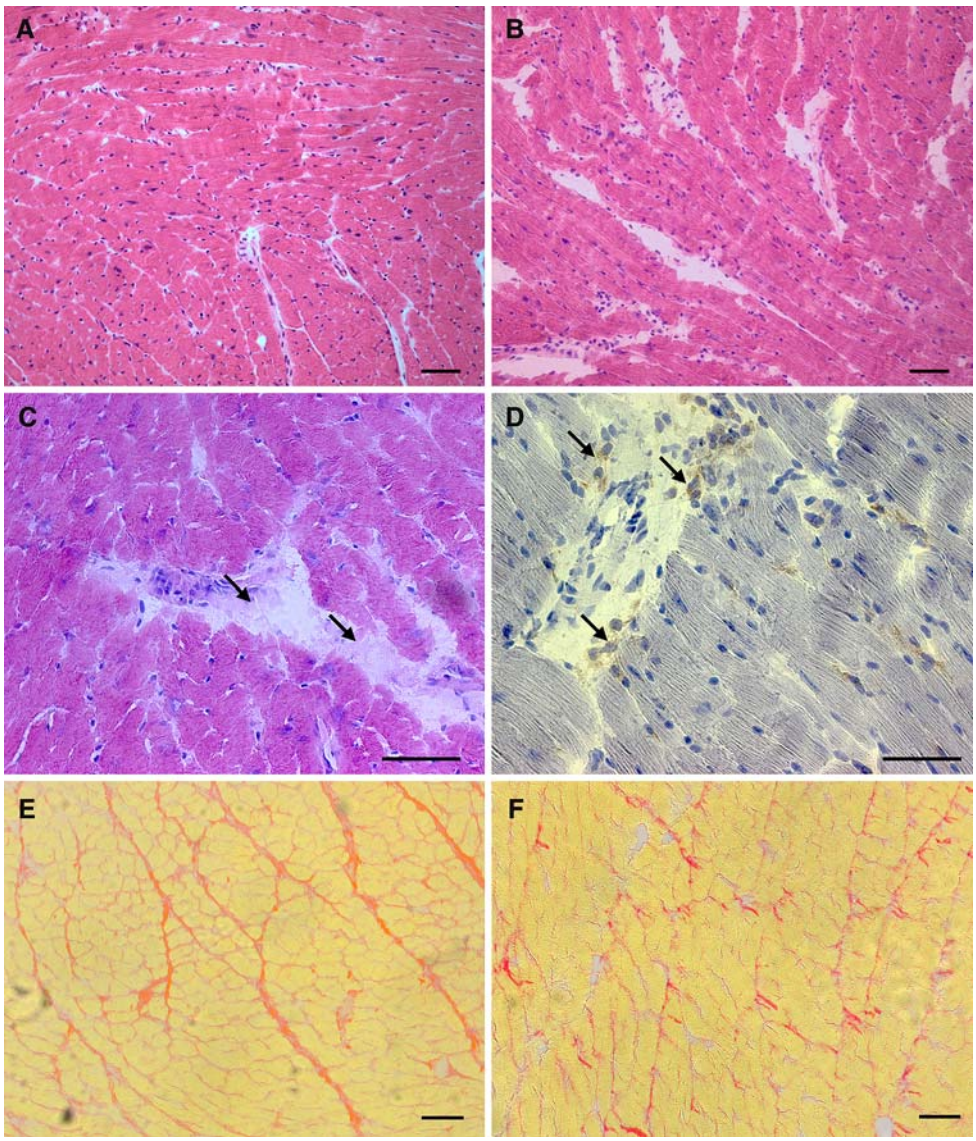

Fig. 4 Morphological alterations of left ventricular cardiac muscle in 70 week DESMUT mice, compared to WT group. Bars correspond to 50 μm. (**a**) Cardiac muscle of WT mouse. Normal myocardial structure, (**b**) Cardiac muscle of DESMUT mouse. Disorganization of overall tissue architecture and increased cellularity, (**c**) Cardiac muscle of DESMUT mouse. Note cellular infiltration and depositions of amorphic material (arrows), (**d**) Cardiac muscle of DESMUT mouse. Muscle fibre disruption and cellular infiltration. Positive CD 68 staining in brown indicating macrophage infiltration. (**e**) Sirius red staining of DESMUT mouse cardiac muscle showing increased amount of connective tissue. (**f**) Sirius red staining of WT mouse cardiac muscle

During recovery from fatigue, force was significantly lower ($P < 0.05$) in the soleus of DESMUT animals compared to WT at 5 and 10 min of recovery (Fig. 7c). There were no differences in relative force, fatigue or recovery in the EDL of DESMUT compared to WT mice (data not shown).

SHIRPA test reveals reduced muscle strength in DESMUT mice

A SHIRPA test was performed on all animals as a screening of neuromuscular performance. DESMUT mice were found to differ from their WT counterparts in performances of the wire manoeuvre test, which is an indicator of hind limb muscle strength. Already at the age of 14 weeks there was a tendency in DESMUT mice to perform the wire manoeuvre test worse than WT. At the age of 25 weeks only 36% of DESMUT mice managed to grasp the wire compared with 100% in control group ($P < 0.05$, Fig. 8a). At the age of 40 weeks only 45% of DESMUT mice were able to lift their hind-legs to the wire and 18% able to grasp the wire, compared with 100% and 55% of WT mice, respectively ($P < 0.05$) (Fig. 8b). At the age of 58 weeks only 27% of DESMUT mice were able to lift the hind-legs, compared with 82% in control group ($P < 0.05$) (Fig. 8c). Importantly, in all other tests and parameters (gait, posture, motor control and co-ordination, excitability and aggression, salivation, piloerection and locomotor activity) there were no significant differences between mice from DESMUT and WT groups.

Cardiac function analysis

At the age of 40 weeks, echocardiography revealed a significant increase of left ventricular posterior wall thickness (LVPW) in DESMUT compared to WT mice ($P < 0.05$) (Table 2). Systolic (LVESD) and diastolic (LVEDD)

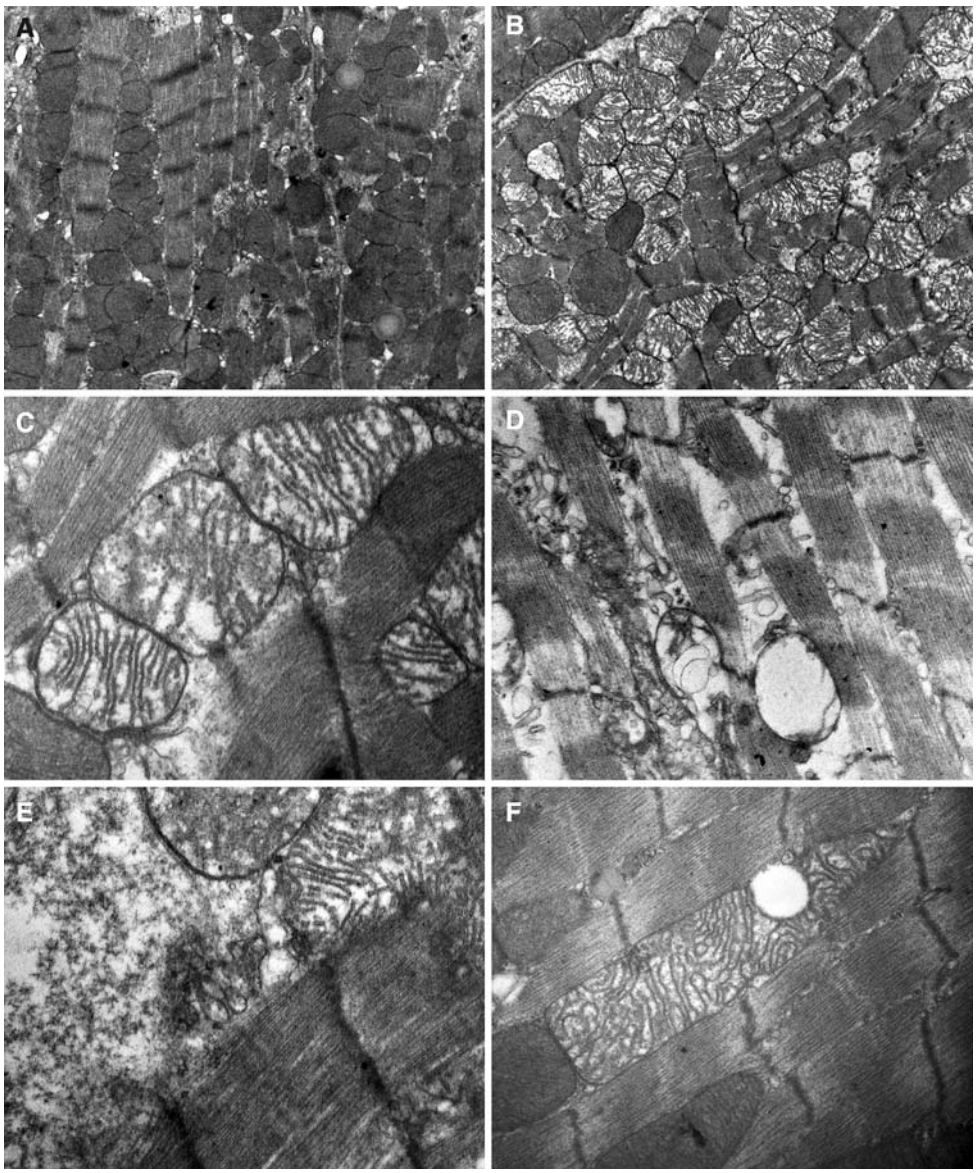

Fig. 5 Electron micrographs of muscle tissue from WT and DESMUT mice. (**a**) Left ventricle sample from 80 weeks old WT mouse. Clusters of dense non-damaged mitochondrias in the intermyofibrillar space, 10,000×. (**b**) Left ventricle sample from 80 weeks old DESMUT mouse. Aggregates of swollen and disrupted mitochondria, alteration of regular myofibril distribution and thinning of myofibrils, 10,000×. (**c**) Left ventricle sample from 80 weeks old DESMUT mouse. Swelling and disruption of mitochondrial matrix, 40,000×. (**d**) Vacuolisation of mitochondrial matrix in tibialis anterior of 80 weeks old DESMUT mouse, 20,000×. (**e**) Left ventricle sample from 80 weeks old DESMUT mouse. Amorphous material, filling intermyofibrillar space close to swollen and disrupted mitochondria, 40,000×. (**f**) Giant mitochondria in left ventricular sample from 80 week old DESMUT mouse, 12,000×

dimensions of left ventricle as well as its contractility as measured by fractional shortening (FS) did not differ between DESMUT mice and the control group. Also at the age of 70 weeks a thickening of the LVPW was noticed in DESMUT mice. At the same time LVEDD was significantly smaller in DESMUT mice ($P < 0.05$), compared to WT mice. There was no significant difference in FS. The PR interval, recorded by ECG, was not significantly different between DESMUT and WT groups.

Discussion

Here we describe a new transgenic mouse model, carrying the L345P mutation of the desmin gene previously shown to cause myopathy and cardiomyopathy in humans (Sjöberg et al. 1999). The aim of our study was to identify muscle changes caused by this mutation. Indeed we found that this model gave us intriguing new information on mutated desmin protein influencing skeletal and heart myocytes in spite of the lack of desmin aggregates seen in patients with the human desminopathy disease.

We utilized a native desmin promoter in order to obtain the most natural profile of L345P desmin expression in various muscle tissues. This promoter has previously been shown to induce GFP expression in muscle cells in culture and to recapitulate expression of endogenous desmin, i.e. not to confer expression in non-muscular tissues (Mericskay et al. 1999). Our results show that the expression profile of L345P desmin in various muscle tissues was highest in heart and diaphragm, i.e. similar to desmin expression in WT animals. We did not observe L345P

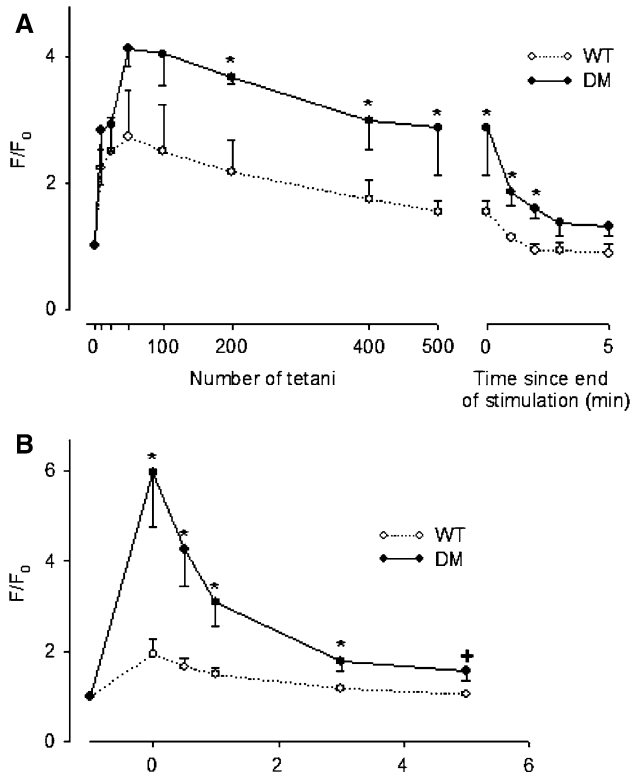

Fig. 6 Mitochondrial Ca^{2+} uptake in skeletal and cardiac myocytes from 70 weeks old animals (**a**) Comparison of mitochondrial Ca^{2+} uptake and release in soleus fibres during and after a series of 500 tetanic contractions at 2 s intervals in WT ($n = 5$) and DESMUT ($n = 3$) cells. F/F_0: relative increase in the fluorescence level. Values are mean ± SEM., $^*P < 0.005$. (**b**) Comparison of mitochondrial Ca^{2+} uptake and release in cardiomyocytes after one min of 1 Hz stimulation in normal Tyrode solution in DESMUT ($n = 10$) cells and WT ($n = 16$) cells. F/F_0: relative increase in the fluorescence level. Values are mean ± SEM. All values significantly different between groups, $^*P < 0.005$ except for 5 min value where $+P < 0.05$

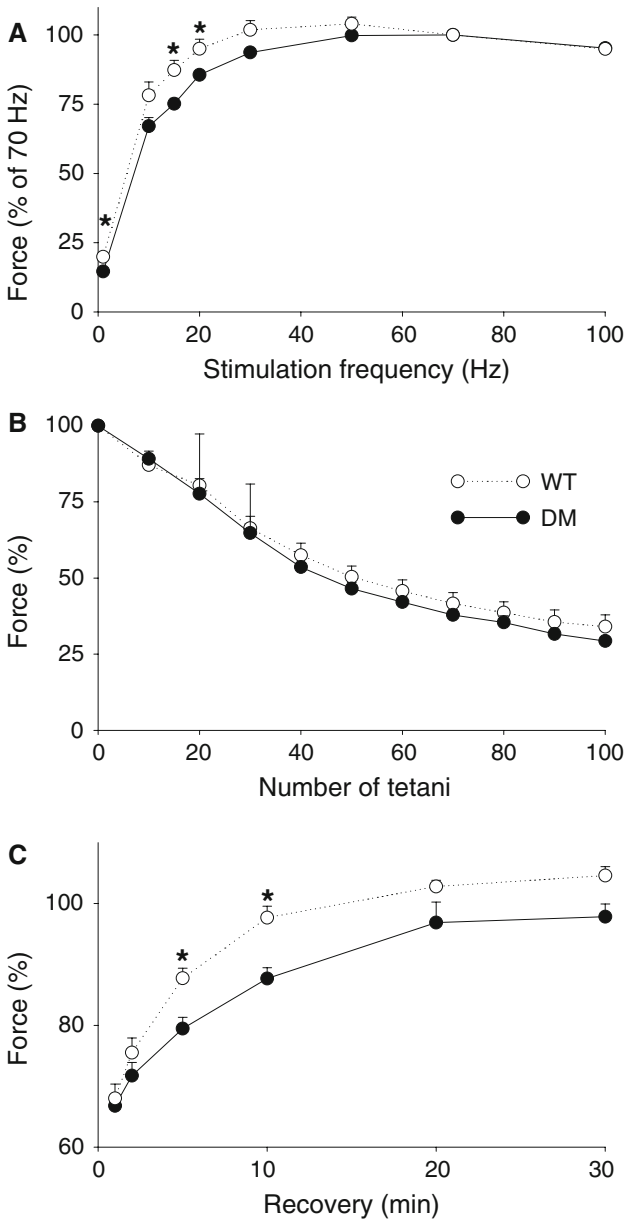

Fig. 7 Contractile function of isolated soleus muscles in 70 weeks old DESMUT and WT animals. All values shown are mean ± SEM, *indicates significant difference between DESMUT ($n = 4$) and WT ($n = 3$) muscles with $P < 0.05$. (**a**) Force frequency curve showing force expressed as a percent of that produced at 70 Hz. (**b**) Tetanic force developed during a series of 100 tetanic contractions at 2 s intervals. (**c**) Recovery of tetanic force during 30 min after the induction of fatigue

desmin protein in urinary bladder, with very low expression in smooth muscles detected by RT-PCR (data not shown), and no protein expression detected by Western blot analyses. This corresponds with data earlier reported by Mericskay et al. that a 4 kb regulatory region controls expression in the heart, skeletal muscles and blood vessels, but is not enough to induce expression in bladder (Mericskay et al. 1999). Consistent with this, we did not find any mechanical alterations in smooth muscles obtained from urinary bladder or micro-arterial vessels from DESMUT mice (data not shown). The average L345P desmin content in the insoluble protein fraction in skeletal and cardiac muscle was low, corresponding to approximately 5% of WT desmin. In line with this, HA-tagged transgenic desmin was undetectable by immunohistochemistry (not presented). The reason for the low level of transgene expression is not clear. However, one likely cause is a relative lack of sufficient regulatory sequences and enhancer elements in the construct, necessary to recapitulate normal activation of the desmin promoter (Gao et al. 1998; Li et al. 1993; Mericskay et al. 2000).

Interestingly, the proportion of L345P desmin to normal desmin in the soluble protein fraction was approximately three times higher than in the insoluble fraction of DESMUT muscle. Under normal physiological conditions, desmin forms highly insoluble polymers (Lazarides 1980,

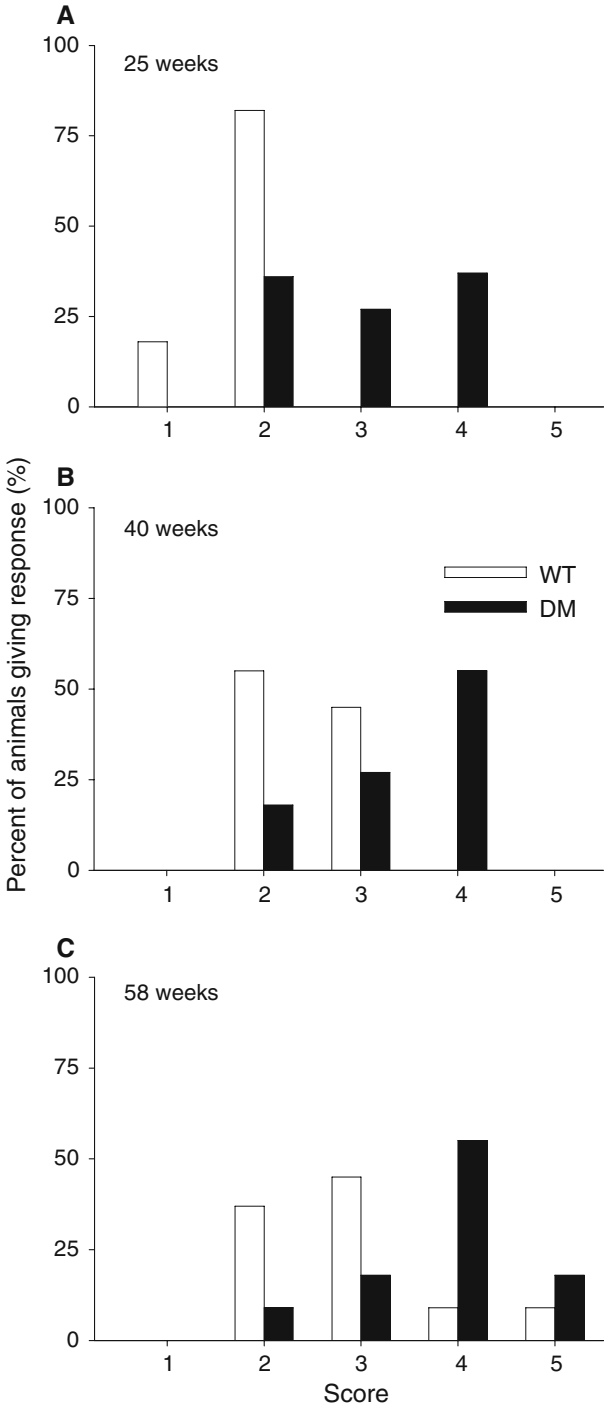

Fig. 8 SHIRPA protocol. Wire Manoeuvre test. Wire manoeuvre activity was graded 1–4: 1, active grip with hind legs; 2, difficulty to grasp with hind legs; 3, unable to grasp with hind legs; 4, unable to lift hind legs; falls within seconds; 5, fall immediately. (**a**) 25 weeks of age. Number of animals: DESMUT = 20, WT = 16; (**b**) 40 weeks of age, Number of animals: DESMUT = 20, WT = 16; (**c**) 58 weeks of age, Number of animals: DESMUT = 11, WT = 11

1982). It was shown previously that L345P mutant desmin, as well as several other mutant desmin isoforms, are not able to polymerize properly (Bär et al. 2005; Sjöberg et al. 1999; Sugawara et al. 2000), and this is the most likely explanation of the higher abundance of mutant desmin in the non-filamentous soluble fraction.

It was showed that the mixture of the equal ratios of wild type and mutant desmin isoforms leads to the formation of desmin aggregates and collapse of the filamentous network (Bär et al. 2006a, b). In the earlier described model of desmin transgenic mice with 3:1 ratio of the over expressed transgenic desmin to the wild type desmin formation of intracellular desmin aggregates was also detected by electron microscopy and lead to cardiac hypertrophy and functional cardiac alterations (Wang et al. 2001). However, in our study the amount of the transgenic mutant desmin was very low which probably was the reason for the absence of morphological features typically seen in skeletal muscle from humans with desmin L345P mutation. These include IF aggregate formation and myopathic changes with large variability in fibre size and fibre maturation, as well as increased amount of fat and connective tissue (Carlsson et al. 2002).

Despite the low expression of mutant protein and the absence of desmin aggregates there was a striking abnormality in L345P desmin transgenic mice, namely a severe alteration of mitochondrial morphology and Ca^{2+} handling. This was seen both in skeletal and cardiac muscles, suggesting a common mechanism, by which desmin mutation influences mitochondrial integrity in muscle cells. This observation agrees well with data obtained on desmin knock-out mice, where marked changes of mitochondrial morphology, as well as of mitochondrial proteomics and enzyme activity, were reported by several groups (Milner et al. 2000; Fountoulakis et al. 2005; Linden et al. 2001). Together with our data it implies that mitochondrial abnormalities constitute a sensitive sign of compromised desmin cytoskeleton in muscle (Milner et al. 2000). It is important to note that in our study these abnormalities were induced not by absence of desmin, but rather by the presence of low levels of abnormal desmin protein. This suggests that the mitochondrial changes observed in the present study reflects a dominant-negative effect of mutant desmin filaments.

The mechanism leading to alteration of mitochondrial morphology in L345P desmin mice is not clear. It is well known that mitochondrial structure and function are highly dependent on the cytoskeleton (Rappaport et al. 1998). Further, the function of the outer mitochondrial membrane has been reported to be dependant on the cellular cytoskeleton (Kay et al. 1997; Saks et al. 1995). Since desmin is known to play an important role in mitochondrial positioning and function (Capetanaki 2002), we speculate that the altered physical properties and function of desmin filaments due to copolymerization with L345P desmin compromises the outer mitochondrial membrane and leads

Table 2 Echocardiographic parameters of WT and DM

	40 weeks		70 weeks	
	WT ($n = 12$)	DM ($n = 12$)	WT ($n = 5$)	DM ($n = 5$)
Heart/body index (%)	N/A	N/A	0.45 ± 0.03	0.37 ± 0.04*
LVEDD (mm)	3.9 ± 1.2	3.8 ± 1.5	3.9 ± 0.9	3.5 ± 1.5*
LVESD (mm)	2.6 ± 1.3	2.4 ± 1.7	2.6 ± 0.8	2.4 ± 1.8
LVPWd (mm)	0.76 ± 0.03	0.92 ± 0.05*	0.80 ± 0.04	1.03 ± 0.01*
LVPWs (mm)	1.1 ± 0.04	1.3 ± 0.08*	1.2 ± 0.04	1.4 ± 0.01*
FS%	33.4 ± 1.4	35.0 ± 2.2	34.4 ± 2.2	33.4 ± 2.2

Values are mean ± SEM; LVEDD, left ventricular end-diastolic diameter; LVESD, left ventricular end-systolic diameter; LVPWd, left ventricular posterior wall thickness in diastole; LVPWs, left ventricular posterior wall thickness in systole; FS, fractional shortening; N/A, not analyzed; * $P < 0.05$, compared to WT

to the matrix swelling. Several desmin-associated proteins (plectin, synemin and paranemin) have been described as potential linkers between desmin filaments and mitochondria (Reipert et al. 1999). Precisely how the desmin filaments alone, or through linker proteins influence physical and biochemical properties of the outer mitochondrial membrane remains elusive.

Aside from their important role as energy suppliers, mitochondria may also play a role to modulate the cytosolic free [Ca^{2+}]. This has been demonstrated in many tissues including neurons (David et al. 1998), cardiac myocytes (Duchen et al. 1998) and frog skeletal muscle fibres (Lännergren et al. 2001). Our results show that mitochondrial Ca^{2+} uptake is increased, and release slowed, both in skeletal muscle fibres and cardiomyocytes of DESMUT mice, compared to WT. It may be speculated that the greater Ca^{2+} loading of the mitochondria in DESMUT compared to normal mice contributes to the changes seen in DESMUT mice. Ca^{2+} is reported to be a potential stimulator of mitochondrial function, and an increased level of Ca^{2+} stimulation of mitochondrial respiration can lead to formation of reactive oxygen species (ROS) (Brookes et al. 2004). It was reported that formation of ROS due to impaired mitochondrial function might be a trigger of cardiac hypertrophy, mitochondrial-induced metabolic cardiomyopathy and diabetic cardiomyopathy (Esposito et al. 1999; Russell et al. 2005; Ye et al. 2004). This process was described in several mouse models of mitochondrial dysfunction (Russell et al. 2005). Altered mitochondrial function together with formation of ROS might also results in the poor recovery of soleus after fatigue. Mouse soleus normally predominantly consists of slow oxidative type I muscle fibers highly dependent on mitochondrial function. For this reason it seems reasonable that soleus muscle is the muscle type most compromised in DESMUT mice. However the reason for such selective injury of slow oxidative muscle fibers remains unknown. The impaired force generation in skeletal muscles from DESMUT mice can partly explain their bad performance in SHIRPA protocol.

In conclusion, we present a mouse model with a mild desminopathy due to transgenic expression of L345P mutated desmin protein. We found that the L345P desmin has a dominant negative function in skeletal and cardiac muscles even at very low level of expression. The primary effect of the mutated desmin appears not to be on the force generation per se (i.e. sarcomere contraction and force transmission through the cytoskeletal filaments), but rather on the mitochondrial structure and altered Ca^{2+} handling.

Acknowledgements We acknowledge the skilled technical assistance of Ann-Christin Thelander. This work was supported by the Swedish Heart-Lung foundation, Stiftelsen Frimurare Barnhuset, King Gustav V and Queen Victoria foundation, Sällskapet Barnavård, Stiftelsen Samariten, Ronald MacDonald Child Fund, Sunnerdahls Handikappfond, Swedish Research Council and Swedish Institute (KIRT program), and United Mitochondrial Disease Foundation.

References

Bär H, Mucke N, Kostareva A et al (2005) Severe muscle disease-causing desmin mutations interfere with in vitro filament assembly at distinct stages. Proc Natl Acad Sci USA 102:15099–15104. doi:10.1073/pnas.0504568102

Bär H, Kostareva A, Sjoberg G et al (2006a) Forced expression of desmin and desmin mutants in cultured cells: impact of myopathic missense mutations in the central coiled-coil domain on network formation. Exp Cell Res 312:1554–1565. doi:10.1016/j.yexcr.2006.01.021

Bär H, Mucke N, Ringler P et al (2006b) Impact of disease mutations on the desmin filament assembly process. J Mol Biol 360:1031–1042. doi:10.1016/j.jmb.2006.05.068

Barohn RJ (1993) Distal myopathies and dystrophies. Semin Neurol 13:247–255

Belluardo N, Westerblad H, Mudo G et al (2001) Neuromuscular junction disassembly and muscle fatigue in mice lacking neurotrophin-4. Mol Cell Neurosci 18:56–67. doi:10.1006/mcne.2001.1001

Bernardi P (1999) Mitochondrial transport of cations: channels, exchangers, and permeability transition. Physiol Rev 79:1127–1155

Brookes PS, Yoon Y, Robotham JL et al (2004) Calcium, ATP, and ROS: a mitochondrial love-hate triangle. Am J Physiol Cell Physiol 287:C817–C833. doi:10.1152/ajpcell.00139.2004

Bruton J, Tavi P, Aydin J et al (2003) Mitochondrial and myoplasmic [Ca2+] in single fibres from mouse limb muscles during repeated tetanic contractions. J Physiol 551:179–190. doi:10.1113/jphysiol.2003.043927

Capetanaki Y (2002) Desmin cytoskeleton: a potential regulator of muscle mitochondrial behavior and function. Trends Cardiovasc Med 12:339–348. doi:10.1016/S1050-1738(02)00184-6

Carlsson L, Fischer C, Sjoberg G et al (2002) Cytoskeletal derangements in hereditary myopathy with a desmin L345P mutation. Acta Neuropathol 104:493–504

Chen F, Chang R, Trivedi M et al (2003) Caspase proteolysis of desmin produces a dominant-negative inhibitor of intermediate filaments and promotes apoptosis. J Biol Chem 278:6848–6853. doi:10.1074/jbc.M212021200

David G, Barrett JN, Barrett EF (1998) Evidence that mitochondria buffer physiological Ca2+ loads in lizard motor nerve terminals. J Physiol 509(Pt 1):59–65. doi:10.1111/j.1469-7793.1998.059bo.x

Duchen MR, Leyssens A, Crompton M (1998) Transient mitochondrial depolarizations reflect focal sarcoplasmic reticular calcium release in single rat cardiomyocytes. J Cell Biol 142:975–988. doi:10.1083/jcb.142.4.975

Esposito LA, Melov S, Panov A et al (1999) Mitochondrial disease in mouse results in increased oxidative stress. Proc Natl Acad Sci USA 96:4820–4825. doi:10.1073/pnas.96.9.4820

Fauconnier J, Lanner JT, Zhang SJ et al (2005) Insulin and inositol 1,4,5-trisphosphate trigger abnormal cytosolic Ca2+ transients and reveal mitochondrial Ca2+ handling defects in cardiomyocytes of ob/ob mice. Diabetes 54:2375–2381. doi:10.2337/diabetes.54.8.2375

Fidzianska A, Drac H, Kaminska AM (1999) Familial inclusion body myopathy with desmin storage. Acta Neuropathol 97:509–514. doi:10.1007/s004010051021

Fidzianska A, Kotowicz J, Sadowska M et al (2005) A novel desmin R355P mutation causes cardiac and skeletal myopathy. Neuromuscul Disord 15:525–531. doi:10.1016/j.nmd.2005.05.006

Fountoulakis M, Soumaka E, Rapti K et al (2005) Alterations in the heart mitochondrial proteome in a desmin null heart failure model. J Mol Cell Cardiol 38:461–474. doi:10.1016/j.yjmcc.2004.12.008

Gao J, Li Z, Paulin D (1998) A novel site, Mt, in the human desmin enhancer is necessary for maximal expression in skeletal muscle. J Biol Chem 273:6402–6409. doi:10.1074/jbc.273.11.6402

Goldfarb LG, Vicart P, Goebel HH et al (2004) Desmin myopathy. Brain 127:723–734. doi:10.1093/brain/awh033

Herrmann H, Strelkov SV, Feja B et al (2000) The intermediate filament protein consensus motif of helix 2B: its atomic structure and contribution to assembly. J Mol Biol 298:817–832. doi:10.1006/jmbi.2000.3719

Ingber DE (1997) Tensegrity: the architectural basis of cellular mechanotransduction. Annu Rev Physiol 59:575–599. doi:10.1146/annurev.physiol.59.1.575

Kay L, Li Z, Mericskay M et al (1997) Study of regulation of mitochondrial respiration in vivo. An analysis of influence of ADP diffusion and possible role of cytoskeleton. Biochim Biophys Acta 1322:41–59. doi:10.1016/S0005-2728(97)00071-6

Länneergren J, Westerblad H, Bruton JD (2001) Changes in mitochondrial Ca2+ detected with Rhod-2 in single frog and mouse skeletal muscle fibres during and after repeated tetanic contractions. J Muscle Res Cell Motil 22:265–275. doi:10.1023/A:1012227009544

Lazarides E (1980) Desmin and intermediate filaments in muscle cells. Results Probl Cell Differ 11:124–131

Lazarides E (1982) Intermediate filaments: a chemically heterogeneous, developmentally regulated class of proteins. Annu Rev Biochem 51:219–250. doi:10.1146/annurev.bi.51.070182.001251

Li Z, Marchand P, Humbert J et al (1993) Desmin sequence elements regulating skeletal muscle-specific expression in transgenic mice. Development 117:947–959

Li D, Tapscoft T, Gonzalez O et al (1999) Desmin mutation responsible for idiopathic dilated cardiomyopathy. Circulation 100:461–464

Linden M, Li Z, Paulin D et al (2001) Effects of desmin gene knockout on mice heart mitochondria. J Bioenerg Biomembr 33:333–341. doi:10.1023/A:1010611408007

Mericskay M, Li Z, Paulin D (1999) Transcriptional regulation of the desmin and SM22 genes in vascular smooth muscle cells. Curr Top Pathol 93:7–17

Mericskay M, Parlakian A, Porteu A et al (2000) An overlapping CArG/octamer element is required for regulation of desmin gene transcription in arterial smooth muscle cells. Dev Biol 226:192–208. doi:10.1006/dbio.2000.9865

Milner DJ, Mavroidis M, Weisleder N et al (2000) Desmin cytoskeleton linked to muscle mitochondrial distribution and respiratory function. J Cell Biol 150:1283–1298. doi:10.1083/jcb.150.6.1283

Munoz-Marmol AM, Strasser G, Isamat M et al (1998) A dysfunctional desmin mutation in a patient with severe generalized myopathy. Proc Natl Acad Sci USA 95:11312–11317. doi:10.1073/pnas.95.19.11312

Rafael JA, Nitta Y, Peters J et al (2000) Testing of SHIRPA, a mouse phenotypic assessment protocol, on Dmd(mdx) and Dmd(mdx3cv) dystrophin-deficient mice. Mamm Genome 11:725–728. doi:10.1007/s003350010149

Rappaport L, Oliviero P, Samuel JL (1998) Cytoskeleton and mitochondrial morphology and function. Mol Cell Biochem 184:101–105. doi:10.1023/A:1006843113166

Reipert S, Steinbock F, Fischer I et al (1999) Association of mitochondria with plectin and desmin intermediate filaments in striated muscle. Exp Cell Res 252:479–491. doi:10.1006/excr.1999.4626

Russell LK, Finck BN, Kelly DP (2005) Mouse models of mitochondrial dysfunction and heart failure. J Mol Cell Cardiol 38:81–91. doi:10.1016/j.yjmcc.2004.10.010

Saks VA, Kuznetsov AV, Khuchua ZA et al (1995) Control of cellular respiration in vivo by mitochondrial outer membrane and by creatine kinase. A new speculative hypothesis: possible involvement of mitochondrial–cytoskeleton interactions. J Mol Cell Cardiol 27:625–645. doi:10.1016/S0022-2828(08)80056-9

Sjöberg G, Saavedra-Matiz CA, Rosen DR et al (1999) A missense mutation in the desmin rod domain is associated with autosomal dominant distal myopathy, and exerts a dominant negative effect on filament formation. Hum Mol Genet 8:2191–2198. doi:10.1093/hmg/8.12.2191

Strelkov SV, Herrmann H, Geisler N et al (2002) Conserved segments 1A and 2B of the intermediate filament dimer: their atomic structures and role in filament assembly. EMBO J 21:1255–1266. doi:10.1093/emboj/21.6.1255

Sugawara M, Kato K, Komatsu M et al (2000) A novel de novo mutation in the desmin gene causes desmin myopathy with toxic aggregates. Neurology 55:986–990

Wang X, Osinska H, Dorn GW et al (2001) Mouse model of desmin-related cardiomyopathy. Circulation 103:2402–2407

Ye G, Metreveli NS, Donthi RV et al (2004) Catalase protects cardiomyocyte function in models of type 1 and type 2 diabetes. Diabetes 53:1336–1343. doi:10.2337/diabetes.53.5.1336